# Multiphase combustion synthesis and enhanced performance of LiMn$_2$O$_4$ nanoparticles using CNTs as a fuel

## Xiaolong Xie[1], Xiaomei Wang[1]*, Qingtang Zhang[2] and Fuling Tang[1]*

LiMn$_2$O$_4$ nanoparticles were successfully prepared using suitable dosage carbon nanotubles (CNTs) as a fuel through multiphase combustion synthesis. The effects of CNTs on the structure and electrochemical performance of LiMn$_2$O$_4$ were investigated. Rate performance test demonstrates that CNTs dosage greatly affect the electrochemical behaviour of LiMn$_2$O$_4$ and LiMn$_2$O$_4$ prepared by choosing suitable CNTs dosage (7%) as a fuel (C7%-LMO) shows high rate charge–discharge capability. X-ray diffraction results indicate that C7%-LMO has the smallest distortion degree in the crystal, compared to LiMn$_2$O$_4$ prepared without CNTs (C0%-LMO) and LiMn$_2$O$_4$ prepared with 10% CNTs (C10%-LMO). SEM results reveal that the average particle size of C7%-LMO is about 100 nm, which is the smallest among the three samples (C0%-LMO, C7%-LMO and C10%-LMO). This unique microscopic features guarantee C7%-LMO possesses the highest discharge capacity, the best cycling performance and the lowest charge transfer resistance among the three samples.

**Keywords:** Lithium manganese oxide, Electrochemical property, Multiphase combustion synthesis, Lithium ion battery

## Introduction

With the development of lithium ion batteries, low-cost electrode materials have attracted more and more attention.[1–8] Spinel LiMn$_2$O$_4$ has been intensively investigated as the most competitive cathode material for lithium ion batteries, because of its high security, abundant Mn resource, low-cost and environmental benignity.[5–10] Spinel LiMn$_2$O$_4$ has been widely used for large-scale lithium ion batteries in electric vehicles. However, spinel LiMn$_2$O$_4$ suffers from drawbacks like serious capacity fading, which might due to the Jahn–Teller distortion of Mn$^{3+}$ ions, nonuniform distribution of lithium ion within the host,[7] loss of crystallinity and development of microstrain. Preparing LiMn$_2$O$_4$ with reduced particle size is an effective way to mitigate these intrinsic drawbacks. Thus, many efforts have been devoted in preparing LiMn$_2$O$_4$ with reduced particle size.[5,10–16]

Solution combustion synthesis is a common technique to synthesize ultrafine or nanosize materials such as metals and oxides, because of its simplicity, low-cost and energy-effectiveness.[9] For LiMn$_2$O$_4$, solution combustion synthesis can be conducted at comparatively low temperatures for a short period because of the homogeneous distribution of Li, Mn and O at the atomic–molecular level.[10] In a typical solution combustion synthesis of LiMn$_2$O$_4$, metal nitrate oxidant (LiNO$_3$ and Mn(NO$_3$)$_2$) and other suitable fuel reductant such as urea,[11–14] poly(acrylic acid),[15] poly vinyl alcohol,[16] urea and citric acid,[17] glycol and citric acid,[18–20] triethanolamine,[21]

hexamethylenetetramine[22] as well as acetate[23] are both needed to promote auto-ignition. After the auto-ignited combustion at 250–500 °C, nanopowder precursor is obtained and then the precursor is calcinated at 700–800 °C to get the final spinel LiMn$_2$O$_4$.[12–22] Generally, soluble fuel and metal nitrate oxidant are usually necessary to promote auto-ignition by solution combustion synthesis. However, to the best of our knowledge, multiphase combustion synthesis using insoluble fuel has not been investigated up to now. Here, we use carbon nanotubes (CNTs) as an insoluble fuel to prepare LiMn$_2$O$_4$ particles through multiphase combustion synthesis. CNTs are composed of concentrically nested multiple graphene sheets with interlayer distances similar to those of graphite.[24] CNTs, which have been widely utilized in electrode for lithium ion batteries to obtain improved electrochemical performance,[25–27] have many advantages like one-dimensional tube, better crystallinity and thermal conductivity. In consideration of their concentrically nested multiple graphene sheets and one-dimensional tubes, they may be the ideal fuel for multiphase combustion synthesis of LiMn$_2$O$_4$ and other cathode materials.

In this work, Li, Mn and O are homogeneous distributed at the atomic–molecular level and CNTs are uniformly dispersed in the solution as an insoluble fuel. And, then the multiphase mixtures are auto-ignited to prepare LiMn$_2$O$_4$ nanoparticles. Therefore, just like solution combustion synthesis, this multiphase combustion synthesis also has advantage of homogeneous distribution. In addition, CNTs, which can also play the role of structure tuning agent, greatly affect the structure and the electrochemical performance of LiMn$_2$O$_4$. So, we hope LiMn$_2$O$_4$ nanoparticles with enhanced performance can be obtained using CNTs as an insoluble fuel.

[1]School of Material Science and Engineering, Lanzhou University of Technology, Lanzhou, China
[2]School of Petrochemical Engineering, Lanzhou University of Technology, Lanzhou, China

*Corresponding authors, email wxmei06@163.com (X. Wang); tfl03@mails.tsinghua.edu.cn (F. Tang)
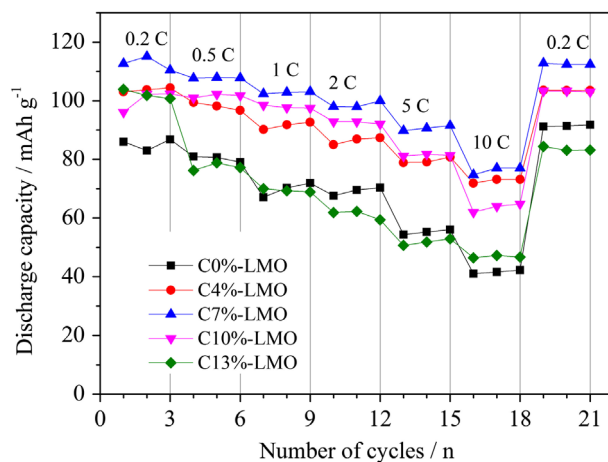
**1 The rate performance of LiMn$_2$O$_4$ sample prepared with different CNTs dosages**

## Experimental

CNTs (50–70 nm) were provided by Chengdu Institute of Organic Chemistry, Chinese Academy of Sciences. The CNTs were soaked in 6 mol/L HNO$_3$ at 90 °C for 3 h and washed by deionized water for several times. Then, CNTs was dried at 60 °C for 12 h in a vacuum oven. LiNO$_3$ (Aladdin, Shanghai) and 50% Mn(NO$_3$)$_2$ solution (Aladdin, Shanghai) were used as the starting materials. All the chemicals were analytical grade. In a typical synthesis of LiMn$_2$O$_4$, 0.03 mol LiNO$_3$, 0.06 mol Mn(NO$_3$)$_2$ was dissolved into ethanol. Different dosage of CNTs was dispersed in ethanol under ultrasonic treatment. Then, the two solutions were mixed together and some solvents were evaporated to get thick suspension. The dark thick suspension was heated to about 250 °C for auto-ignition, and then the grey precursor was gotten. The precursor was grinded and then calcined at 700 °C for 8 h in an air filled muffle furnace. According to the theoretical yield of LiMn$_2$O$_4$, the mass ratios of CNTs/(CNTs + LiMn$_2$O$_4$) were controlled to be 0, 4, 7, 10 and 13 wt.%. Thus, the final LiMn$_2$O$_4$ samples prepared by using different CNTs content were designated as C0%-LMO, C4%-LMO, C7%-LMO, C10%-LMO and C13%-LMO, respectively.

X-ray diffraction (XRD) was performed using a Rigaku RINT2000 X-ray diffractometer over with Cu $K_\alpha$ radiation ($\lambda$ = 0.154 nm) to determine the crystalline structure of C0%-LMO, C7%-LMO and C10%-LMO. The scanning angle $2\theta$ was ranged from 10° to 90° with a rate of 4° ($2\theta$) min$^{-1}$. Scanning electron microscope (SEM JEOL-6301F) was used to exa ine the morphology of the precursors and prepared LiMn$_2$O$_4$ samples.

80 wt.% as prepared LiMn$_2$O$_4$ samples were mixed with 10 wt.% Super P carbon black and 10 wt.% aqueous LA132 binder (Chengdu Indigo power sources CO., Ltd.) in an agate mortar to prepare the viscous slurry, respectively. Then, the slurry was coated on a 20-μm aluminium foil. The coated aluminium foil was split to 12-mm circular dicks (composite cathode). Subsequently, the composite cathode was weighed after drying in a vacuum oven at 100 °C for 8 h. Coin-type CR2032 cells were assembled using the weighed composite cathode, lithium flake anode, Celgard 2400 separator and electrolyte in an argon-filled glove box. The LBC3045i electrolyte is 1 mol/L LiPF$_6$ dissolved in a mixture of ethylene carbonate/dimethyl carbonate/ethyl–methyl carbonate (EC/DMC/EMC is in a volume ratio of 1:1:1), which is purchased from Shenzhen Capchem Chemicals. Galvanostatic charge–discharge tests of the assembled cells were performed at a LAND CT2001A battery testing system (Wuhan

LAND Electronics Co., Ltd.) at room temperature between the voltage ranges of 3.3–4.4 V. The electrochemical impedance spectra (EIS) measurements of the cells after cycling performance test were carried out using a CHI660D electrochemical workstation (Shanghai Chenhua Instruments Co., China). The frequency is in the range of 0.01 Hz–100 kHz with an amplitude of 0.005 V.

## Results and discussion

### Effect of the CNTs dosage on the performance of LiMn$_2$O$_4$

In order to evaluate the CNTs dosage on the performance of LiMn$_2$O$_4$ samples, the five samples are all charged–discharged at enhanced rates. The results are presented in Fig. 1. Clearly, the rate performance of C7%-LMO is the highest among the five samples. At the rate of 0.2 C, the second discharge capacity of C7%-LMO is 115.1 mAh g$^{-1}$. Even at the rate of 10 C, the discharge capacity of C7%-LMO is still as high as 77.0 mAh g$^{-1}$. When the rate changes from 10 C to 0.2 C, C7%-LMO roughly restores its original value. The rate performance of C0%-LMO is the lowest among the five samples. The rate performance of C13%-LMO is as poor as that of C0%-LMO. The rate performance of C4%-LMO is nearly close to that of C10%-LMO and they are both better than C0%-LMO. Therefore, the dosage of CNTs greatly influences the rate performance of LiMn$_2$O$_4$ samples and LiMn$_2$O$_4$ with high rate performance can be achieved with suitable dosage of CNTs. In the following text, C0%-LMO, C7%-LMO and C10%-LMO were chosen as representatives to evaluate the dosage of CNTs on the performance of LiMn$_2$O$_4$ samples.

### XRD analysis

XRD patterns of C0%-LMO, C7%-LMO and C10%-LMO are shown in Fig. 2. All diffraction peaks can be indexed by a cubic spinel structure with Fd3 m space group.[23] Very weak peaks of Mn$_2$O$_3$ are detected for C0%-LMO. It might be that little MnO$_2$ in the sample change to Mn$_2$O$_3$ and O$_2$ above 600 °C. The $I_{(311)}/I_{(400)}$ peak intensity ratio ($R$) reflects the degree of tetragonal distortion in the cubic spinel structure.[6] As shown in Fig. 2, R of C7%-LMO is 0.910, which is much lower than that of C0%-LMO (1.112) and C10%-LMO (1.011). This phenomenon indicates that C7%-LMO has the smallest distortion degree in LiMn$_2$O$_4$ crystal among the three
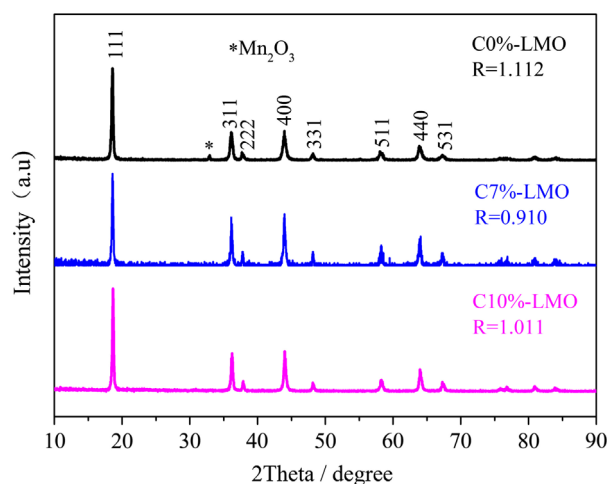
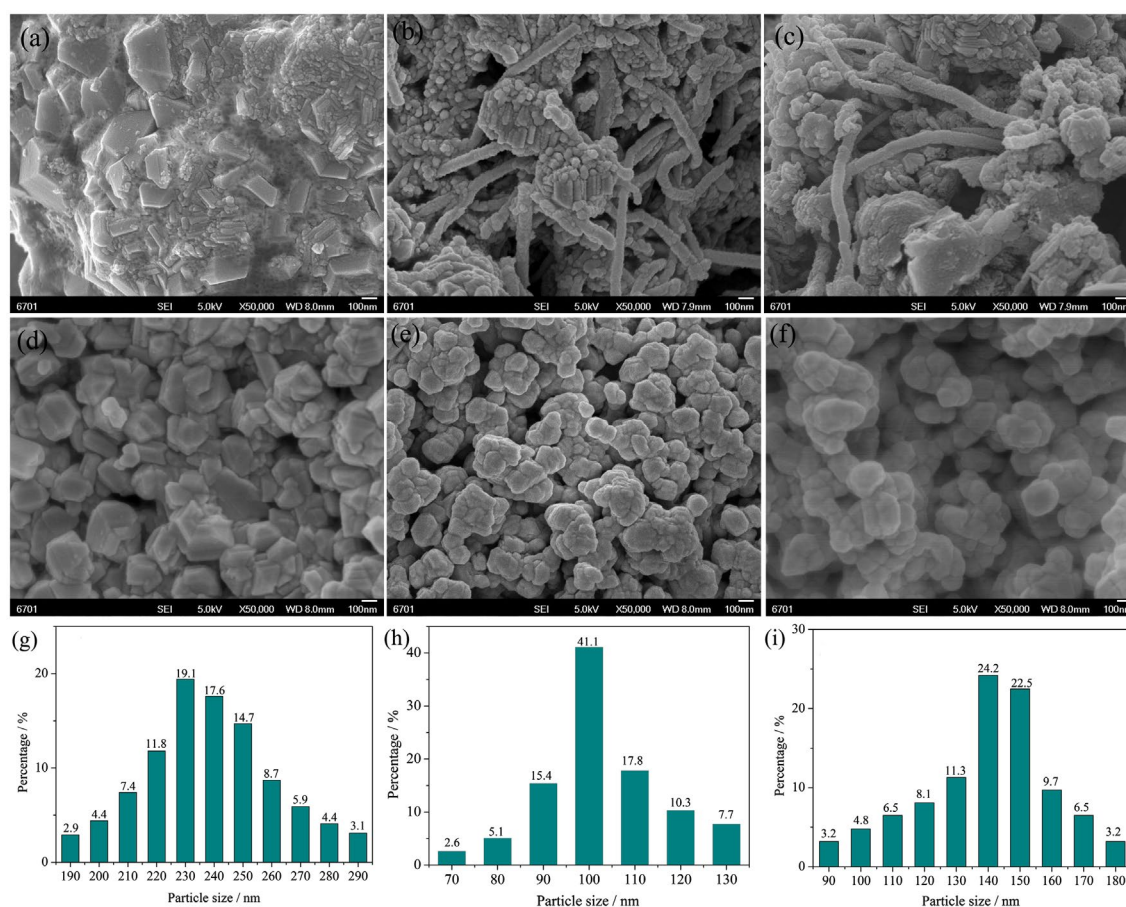**2 XRD patterns of C0%-LMO, C7%-LMO and C10%-LMO**

samples. Therefore, it can be expected that multiphase combustion synthesis of $LiMn_2O_4$ using CNTs as a fuel should exhibit a good electrochemical performance.

## SEM analysis of the precursor and $LiMn_2O_4$ samples

The fluffy precursors and final products of C0%-LMO, C7%-LMO as well as C10%-LMO were examined by SEM and the results are shown in Fig. 3. Figure 3a shows that the precursor of C0%-LMO is mainly composed of tightly contacted large size of particles with 200–300 nm. The large precursor particles might be ascribing to that metal salts decompose at high temperature with no fuel. Figure 3b indicates that the precursor of C7%-LMO is mainly made up of small size of particles about 50 nm and there are also some residual CNTs which are not burned in the auto-ignition. Figure 3c reveals that C10%-LMO is composed of few large size particles with 200–300 nm and many small size particles under 100 nm. In addition, there are also some residual CNTs. These imply that small precursor nanoparticles could be only obtained using suitable dosage CNTs (For instance: 7%), because appropriate ratio of oxide to fuel is necessary for drastic ignition.

As shown in Fig. 3d, C0%-LMO is composed of primary particles with irregular shapes. The particle sizes of C0%-LMO were analysed from Fig. 3d and the result is shown in Fig. 3g. C0%-LMO has a size within the range of 190–290 nm, mainly between 220 and 250 nm. From Fig. 3e, we can find that C7%-LMO is composed of primary particle with spherical shapes and there are no residual CNTs in C7%-LMO particles, indicating CNTs has been burned during the calcination step at 700 °C. The particle sizes of C7%-LMO were also analysed from Fig. 3e and the result is shown in Fig. 3h. C7%-LMO has a size within the range from 70–130 nm, mainly between 90 and 110 nm. Therefore, C7%-LMO is a typical nanoparticles. As shown in Fig. 3f, the morphology of C10%-LMO is similar to that of C7%-LMO. However, C10%-LMO has larger size particles compared to C7%-LMO. As shown in Fig. 3i, C10%-LMO has a size within the range from 90 to 180 nm, mainly between 130 and 150 nm. These results illustrated that the particle size of $LiMn_2O_4$ is roughly in accord with their precursors.
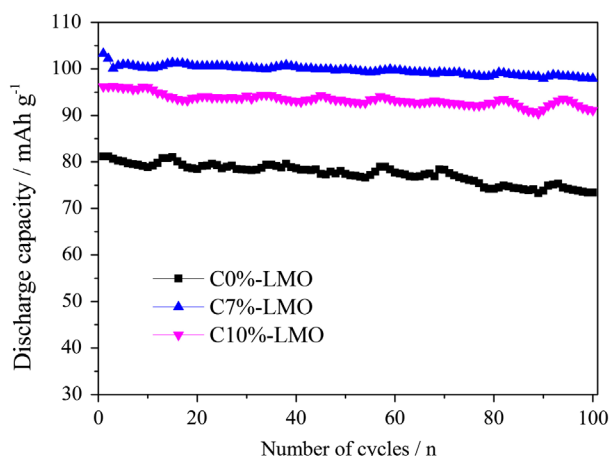


**3 SEM images of the fluffy precursors of C0%-LMO *a*, C7%-LMO *b* and C10%-LMO *c*. SEM images of C0%-LMO *d*, C7%-LMO *e* and C10%-LMO *f*. Particle size distributions of C0%-LMO *g*, C7%-LMO *h* and C10%-LMO *i* analysed from SEM images**
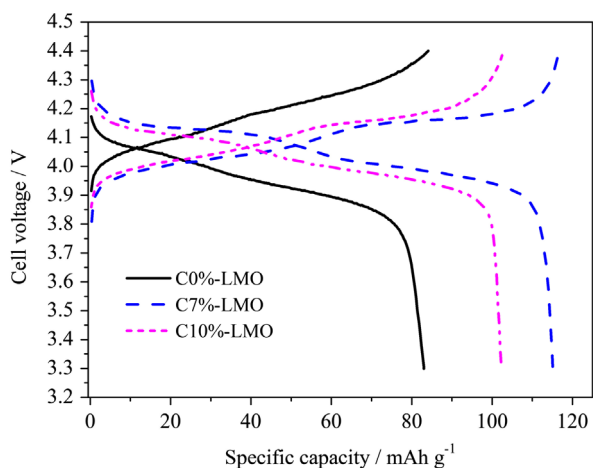
**4 Charge-discharge curves of 0%-LMO, C7%-LMO and C10%-LMO at a current rate of 0.2 C**
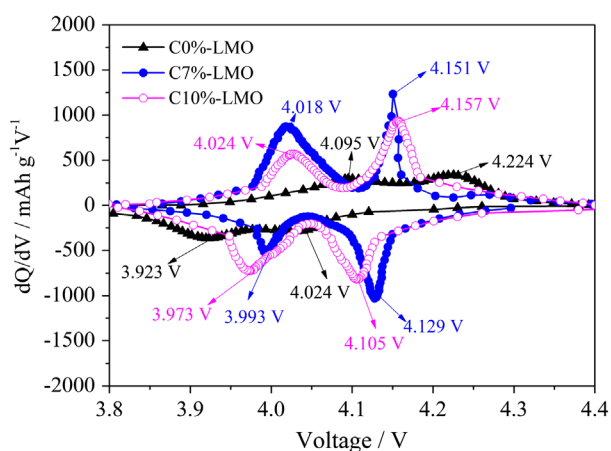


**5 Curves of d$Q$/d$V$ vs. voltage at 0.2 C of C0%-LMO, C7%-LMO and C10%-LMO**



**6 Cycling performance of C0%-LMO, C7%-LMO and C10%-LMO at a current rate of 1 C**

## Electrochemical measurements

The second charge–discharge voltage profiles of the three samples are compared in Fig. 4. All samples are

charged–discharged between 3.3 and 4.4 V at a current rate of 0.2 C. The discharge capacities of C0%-LMO, C7%-LMO and C10%-LMO are 83.0, 115.1 and 102.3 mAh g$^{-1}$, repectively. Compared with the other two samples prepared using CNTs, C0%-LMO shows much higher charge voltage plateau and much lower discharge voltage plateau. While, C7%-LMO exhibits the lowest charge voltage plateau and highest discharge voltage plateau. The smallest difference between charge and discharge plateaus means that internal resistance of C7%-LMO cell is the lowest among the three samples.[10] This might be associated with that nanoparticles of C7%-LMO can shorten the lithium diffuse length, ensuring smaller difference of charge–discharge plateau and larger charge–discharge capacity.

The curves of d$Q$/d$V$ vs. voltage can more clearly reflect oxidation and deoxidization peaks of the electrode materials. Thus, the curves of d$Q$/d$V$ vs. voltage at 0.2 C of C0%-LMO, C7%-LMO and C10%-LMO are presented in Fig. 5. The curves of C0%-LMO exhibit two weak wide anodic peaks and two weak wide cathodic peaks, indicating that the polarization of C0%-LMO is comparatively serious. The redox peaks of the other two samples are clearly observed in Fig. 5. Two anodic peaks at ~4.0 and ~4.10 V are responsible for Li extraction from the 8$a$ sites in the crystal lattice and the formation of Li$_{0.5}$Mn$_2$O$_4$ and Li$_{-0.25}$Mn$_2$O$_4$.[10] Two sharp anodic peaks at 4.151 and 4.018 V are clearly observed for C7%-LMO. In addition, two sharp cathodic peaks at 4.129 and 3.993 V are also observed for C7%-LMO. Two anodic peaks of 4.157 and 4.024 V as well as two cathodic peaks of 4.105 and 3.973 V are observed for C10%-LMO. Therefore, the voltage hysteresis of C7%-LMO between the anodic peak and cathodic peak potentials is the lowest among the three samples, which reflects the good reversibility between charge and discharge processes. The results accord with the charge–discharge voltage curves.

The three samples were charged–discharged at a current rate of 1 C for 100 cycles to evaluate the reversible lithium storage capability and the results are presented in Fig. 6. The first specific discharge capacities of C0%-LMO, C7%-LMO and C10%-LMO are 81.2, 103.3 and 96.2 mAh g$^{-1}$, respectively. Their 100th specific discharge capacities are 73.4, 97.9 and 91.1 mAh g$^{-1}$, respectively. Therefore, the capacity retentions of C0%-LMO, C7%-LMO and C10%-LMO are 90.4, 94.8 and 94.7%, respectively. All the capacity retentions of the samples are above 90% and the capacity retention of C7%-LMO is the highest. In addition, the specific discharge capacity of C7%-LMO is much higher than those of C0%-LMO and C10%-LMO. The capacity retention of C10%-LMO is very close to that of C7%-LMO, but C10%-LMO has much lower specific discharge capacity compared to C7%-LMO. Both capacity retention and specific discharge capacity of C0%-LMO are much lower than those of the other two samples. These results indicate that suitable dosage CNTs as a fuel can greatly improve the cycling performance of LiMn$_2$O$_4$ samples.

EIS were performed to investigate the impedance variation of the cell prepared with C0%-LMO, C7%-LMO and C10%-LMO at 3.87 V after rate performance test. An intermediate frequency semicircle and a low-frequency tail were observed for all three samples, which are shown in Fig. 7. The intermediate frequency semicircle is caused by the charge transfer resistance ($R_{ct}$), which is associated with the 'charge transfer reactions' at the interface of the SEI film and oxide electrode charge transfer resistance.[20,23] The low-frequency tail was associated with lithium ion diffusion impedance in active materials. Smaller radius of the semicircle means that smaller $R_{ct}$. $R_{ct}$ of C0%-LMO, C7%-LMO and C10%-LMO
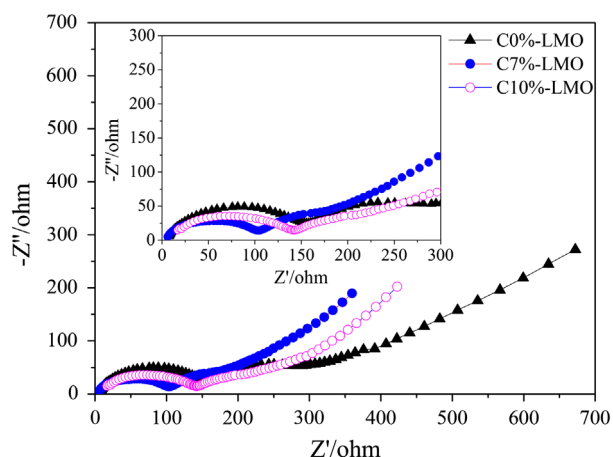
**7 Nyquist plots of cycled cells loaded with C0%-LMO, C7%-LMO and C10%-LMO**

are 150, 100 and 140 $\Omega$, respectively. The lowest $R_{ct}$ of C7%-LMO ensures the best rate capability and the lowest voltage hysteresis in Fig. 5.

The stabilized cycling performance and excellent rate performance of C7%-LMO can be attributed to its unique nanostructure and morphology. Appropriate ratio of oxide to fuel is necessary for drastic ignition, which is essential to prepare nanoparticles.[23,28] So, using suitable dosage of CNTs (7%) can obtain LiMn$_2$O$_4$ nanoparticles. The nanoparticles of C7%-LMO mean short lithium ion diffuse length and therefore C7%-LMO exhibits excellent rate performance. It is well known that preparing LiMn$_2$O$_4$ with reduced particle size is very effective to mitigate the intrinsic drawbacks like serious capacity fading, loss of crystallinity and development of microstrain. Therefore, C7%-LMO exhibits stabilized cycling performance.

## Conclusion

LiMn$_2$O$_4$ nanoparticles were successfully prepared using suitable dosage CNTs as a fuel through multiphase combustion synthesis. Effects of CNTs on the structure and electrochemical performance of LiMn$_2$O$_4$ were investigated. Suitable dosage CNTs used as a fuel can greatly reduce the particle size of the precursor and LiMn$_2$O$_4$ samples. C7%-LMO shows the highest discharge capacity, the best rate performance and the lowest $R_{ct}$ among C0%-LMO, C7%-LMO and C10%-LMO because LiMn$_2$O$_4$ samples with reduced particle size have short lithium diffuse distance. C7%-LMO also exhibits

the best cycling performance, including specific capacity and capacity retention ratio.

## Funding

## References

1. K. Li, F. Shu and K. Chen: *Electrochim. Acta*, 2014, **136**, 10–18.
2. K. Li, H. Chen and F. Shua: *RSC Adv.*, 2014, **4**, 36507–36512.
3. K. Li, S. Lin, F. Shua, J. Zhang, K. Chen and D. Xue: *CrystEngComm*, 2014, **16**, 10969–10976.
4. K. Li, F. Shua and J. Zhang: *Ceram. Int.*, 2015, **41**, 6729–6733.
5. Z. Yang, Y. Jiang, H. H. Xu and Y. H. Huang: *Electrochim. Acta*, 2013, **106**, 63–68.
6. B. S. Liu, Z. B. Wang, Y. Zhang, F. D. Yu, Y. Xue, K. Ke and F. F. Li: *J. Alloy. Compd.*, 2015, **622**, 902–907.
7. M. S. Wang, J. Wang, J. Zhang and L. Z. Fan: *Ionics*, 2015, **21**, 27–35.
8. Y. Shang: *Electrochim. Acta*, 2015, **156**, 121–126.
9. W. Wen and J. M. Wu: *RSC Adv.*, 2014, **4**, 58090–58100.
10. Q. Zhang, J. Mei, X. Wang, J. Guo, F. Tang and W. Lu: *J. Alloy. Compd.*, 2014, **617**, 326–331.
11. E. I. Santiago, S. T. Amancio-Filho, P. R. Bueno and L. O. S. Bulhões: *J. Power Sources*, 2001, **97–98**, 447–449.
12. K. M. Lee, H. J. Choi and J. G. Lee: *J. Mater. Sci. Lett.*, 2001, **20**, 1309–1311.
13. C. Z. Lu and G. T. Fey: *J. Phys. Chem. Solids*, 2006, **67**, 756–761.
14. W. Yang, G. Zhang, J. Xie, L. Yang and Q. Liu: *J. Power Sources*, 1999, **81–82**, 412–415.
15. H. B. Park, J. Kim and C. W. Lee: *J. Power Sources*, 2001, **92**, 124–130.
16. A. Subramania, N. Angayarkanni and T. Vasudevan: *Mater. Chem. Phys.*, 2007, **102**, 19–23.
17. S. Vivekanandhan, M.Venkateswarlu and N. Satyanarayana: *J. Alloy. Compd.*, 2007, **441**, 284–290.
18. K. Du and H. Zhang: *J. Alloy. Compd.*, 2003, **352**, 250–254.
19. X. Wu, X. Li, Z. Xiao, J. Liu, W. Yan and M. Ma: *Mater. Chem. Phys.*, 2004, **84**, 182–186.
20. X. Wu, S. Chen, Z. He, Z. Xiao, M. Ma and J. Liu: *Ceram. Int.*, 2008, **34**, 1387–1391.
21. G. T. Fey, Y. D. Cho and T. P. Kumar: *Mater. Chem. Phys.*, 2004, **87**, 275–284.
22. G. T. Fey, Y. D. Cho and T. P. Kumar: *Mater. Chem. Phys.*, 2006, **99**, 451–458.
23. Q. Zhang, J. Mei, X. Wang, W. Fan, F. Wang, W. Lu and F. Tang: *J. Alloy. Compd.*, 2014, **606**, 249–253.
24. J. H. Lehman, M. Terrones, E. Mansfield, K. E. Hurst and V. Meunier: *Carbon*, 2011, **49**, 2581–2602.
25. R. Epur, M. K. Datta and P. N. Kumta: *Electrochim. Acta*, 2012, **85**, 680–684.
26. C. Liu, H. Huang, G. Cao and F. Xue: *Electrochim. Acta*, 2014, **144**, 376–382.
27. L. Yang, J. Hu, A. Dong and D. Yang: *Electrochim. Acta*, 2014, **144**, 235–242.
28. Q. Zhang, J. Mei, X. Xie, X. Wang, W. Lu and J. Zhang: *Mater. Res. Bull.*, 2015, **70**, 397–402.